

by the dotted line, and misses the exact result by a factor of two, for $T_c < T < 1.75T_c$, the effective range of observables emerging from SPS and RHIC experiments. The experimental error in determination of α_s is today considerably smaller. This large difference between exact and approximate result arises, in part, because the value of $\Lambda^{(5)}$ used to obtain the thermal behavior was adjusted to be $\Lambda^{(4)} = 0.95T_c \simeq 0.15$ GeV. This value would be correct if T_c were indeed around 210 MeV, as has been thought for some time.

The high sensitivity of physical observables to α_s , makes it imperative that we do not rely on this approximation. Yet a fixed value $\alpha_s = 0.25$ (instead of $\alpha_s = 0.5$) derived from this approximation is still often used in studies of the phase properties of QGP, loss of energy by jets of partons, thermalization of charmed quarks, thermal production of strange quarks, etc. Such a treatment of thermal QCD interaction underestimates by as much as a factor of four the interaction with the QGP phase, and thus the speed of these processes. In most cases, this mundane factor matters, and we see that an accurate evaluation of α_s at the appropriate physical scale is required in order to establish the correct magnitude of these results.

15 Lattice quantum chromodynamics

15.1 The numerical approach

The perturbative approach to QCD lacks the capability to describe the long-distance behavior, which is essential for understanding the QGP–HG transformation. We need a more rigorous approach in order to characterize the physical mechanisms at the origin of color confinement, and the transition to the deconfined state of hadronic matter. A suitable nonperturbative approach is the numerical study of QCD on a lattice (L-QCD).

L-QCD is a vast field that is evolving very actively. We will limit our presentation to a pedestrian guide to the language used in this field, along with a report on a few key results of greatest importance to us. We will not be embarking on a thorough introduction to the theoretical and numerical methods. For a survey of the historical developments until the early eighties we refer to the monograph by Creutz [97], and for a summary of recent theoretical advances, and many numerical results addressing hot QCD, we refer the reader to the recent survey by Karsch [159].

The particular usefulness of the lattice-gauge-theory formulation is that it allows one to numerically carry out Feynman path integrals which represent expectation values of quantum-field-theory operators. Specifically, the expectation value of an operator \mathcal{O} , including both glue and quark

fields, is

$$\langle \mathcal{O} \rangle = \frac{\int [dA_\mu d\bar{\psi} d\psi] \mathcal{O} e^{-i \int \mathcal{L}(A, \bar{\psi}, \psi) d^4x}}{\int [dA_\mu d\bar{\psi} d\psi] e^{-i \int \mathcal{L}(A, \bar{\psi}, \psi) d^4x}}. \quad (15.1)$$

These integrals are over all values of the gluon and quark fields at all points in space and time. However, most parts of the domain of the integral are unimportant – in ‘weak coupling’ (i.e., when perturbative expansion makes good sense), only paths close to the classical paths (classical-field solutions) are important. In order to do a path integral efficiently, it is essential to sample more densely the domains that give large contributions, see Eq. (15.2) below, and this obviously then poses a practical challenge. The integration measure of the path integral is indicated by $[dA_\mu d\bar{\psi} d\psi]$. The goal of computations, in lattice QCD, is to evaluate Eq. (15.1) numerically by evaluating the integrand at selected lattice points representing its domain.

The functional integral in Eq. (15.1), expressed on the lattice, means that we are integrating the fields at each lattice site and lattice link, and the domain of the integral has accordingly a very high dimensionality. The method of choice for doing such integrals numerically is the Monte-Carlo (random-choice) method. However, a considerable complication in applying this method arises since $e^{-i \int \mathcal{L} d^4x}$ is not in general a positive real number: aside from the i factor in the exponent, it is a functional of quark fields, which have to be represented by anticommuting numbers: $\psi_x \psi_y = -\psi_y \psi_x$. This problem can be solved since the dependence on ψ and $\bar{\psi}$ of Eq. (15.1) has the form of a polynomial times a Gaussian. Therefore, the quark portion of the path integral can be done analytically. This integral yields a ‘Fermi determinant’ FD , which changes for each configuration of the gauge (gluon) fields considered. We will address the form of FD in section 15.4.

In order to allow a Monte-Carlo integration procedure for the gauge fields, the explicit i in the exponent in Eq. (15.1) is combined with dt , and the integral is considered in ‘imaginary’ time, or, as it is usually said, Euclidian space. It is generally believed that some, if not all, physical results can be analytically continued from the real- to the imaginary-time axis. Even so, the Fermi determinant remains real only for zero chemical potential, and we can use as a probability for sampling the Monte-Carlo integral

$$\rho(A) = FD_I e^{-\int \mathcal{L}_a d^4x_I}. \quad (15.2)$$

\mathcal{L}_a is the gluon part of the Lagrangian in imaginary time and subscript I indicates that the quantities have been suitably modified by the transformation $t \rightarrow it$.

The physical system is restricted to a finitely sized box, which introduces an infrared (long-distance) cutoff at the size of the box, L . The continuous space and time is represented by a lattice, which introduces an ultraviolet cutoff (i.e., distance) at the lattice spacing[†] ℓ . In going from the continuum to the lattice, derivatives are replaced by finite differences. This replacement must be done in a gauge-invariant way, and hence one often refers to lattice gauge theory (LGT) or, in our context, lattice quantum chromodynamics (L-QCD).

In what follows, we will describe how to deal with dynamic gluons and quarks. Since the presence of quarks requires that the Fermi determinant FD be evaluated, this imposes a need for much more computational effort than in the case of the ‘pure-gauge’ lattice which comprises gluons only. In an intermediate step we can study quark operators in a non-fluctuating gauge-field background; this is the ‘quenched’-quark approximation, which excludes the contributions of particle–antiparticle pairs. The full calculation then has ‘dynamic’ quarks.

15.2 Gluon fields on the lattice

Replacement of continuous space–time x_μ by a lattice $x_\mu = \ell n_\mu$ must be accomplished in a gauge-invariant manner, and, as with any other regulator, in order to be able to interpret the results, the regulator, i.e., lattice spacing, must be removed ($\ell \rightarrow 0$) after a finite result has been obtained. In other words, contact with the real physical world exists only, in the continuum limit, when the lattice spacing is taken to zero; this limit must be reached in natural fashion in any formulation. Moreover, we must always be aware that, on the lattice, we sacrifice Lorentz invariance, and have to be vigilant about the fates of all internal symmetries, which we desire to preserve. A suitable approach was devised by Wilson [273].

The action, an integral over the Lagrangian, is replaced by a sum over sites:

$$\beta S = \int dx \mathcal{L} \rightarrow \ell^4 \sum_n \mathcal{L}_n. \quad (15.3)$$

β reminds us that all calculations are carried out in a four-dimensional Euclidian world, and β corresponds to the time dimension, or, as we shall see for equilibrium thermodynamics, the usual relation $\beta = 1/T$ applies. The generating functional used to obtain many of the results implied by

[†] It is common to call the lattice spacing a . To avoid conflicts of notation with the color indices of QCD, we chose the symbol ℓ , which is not used as often, though it should not be confounded with the angular-momentum eigenvalue employed earlier.

Eq. (15.1) is now an ordinary integral over all lattice fields and sites ϕ_n^i :

$$Z = \int \left(\prod_i \prod_n d\phi_n^i \right) e^{-\beta S}. \quad (15.4)$$

In the specific case of interest to us, quantum chromodynamics, this integral does not comprise the gauge fields A_μ^a ; these are represented by fundamental variables $U_\mu(n)$, which live on the links connecting point x_n and $x_n + \ell\mu$ of a $d = 4$ dimensional space [273],

$$U_\mu(n) \equiv e^{igt^a A_\mu^a(n)}, \quad (15.5)$$

which form arises from Eqs. (13.64) and (13.69). We have $U_\mu(x_n + \ell\mu)^\dagger \equiv U_\mu(n + \mu)^\dagger = U_\mu(x_n) \equiv U_\mu(n)$. t_a are generators of the $SU_c(3)$ gauge group, $U_\mu(n)$ are elements of this group. The quark fields $\Psi(n)$ remain ‘attached’ to the lattice sites x_n ; see below. Under the gauge transformation, the site variables (quark fields) transform as in Eq. (13.65) and link variables, which, as we will see, represent a generalization of field strengths, transform under gauge transformations in generalization of Eq. (13.77),

$$U_\mu(x) \rightarrow V(x)U_\mu(x)V^\dagger(x + \hat{\mu}). \quad (15.6)$$

An action for gauge fields involves a gauge-invariant product of U_μ ’s around some closed contour, a ‘plaquette’. Since, for almost any closed contour, the leading term in the expansion is proportional to $F_{\mu\nu}^2$ in the continuum limit, there is considerable arbitrariness in the definition of gluon lattice action. The simplest contour has a perimeter of four links. In $SU(N)$

$$\beta S^W \equiv \frac{2N}{g^2} \sum_n \sum_{\mu > \nu} \text{Re tr} \{1 - U_\mu(n)U_\nu(n + \hat{\mu})U_\mu^\dagger(n + \hat{\nu})U_\nu^\dagger(n)\}. \quad (15.7)$$

βS^W is called the ‘Wilson action’. The volume element in Eq. (15.4) is simply an integral over the group elements:

$$\left[\prod_i \prod_n d\phi_n^i \right] \rightarrow \left[\prod_n dU_n \right]. \quad (15.8)$$

Summation over all group elements amounts to a projection of the argument in the integral onto its color-singlet component.

15.3 Quarks on the lattice

The Euclidian fermion action in the continuum (in four dimensions) is

$$S = \int d^4x [\bar{\psi}(x)\gamma^\mu \partial_\mu \psi(x) + m\bar{\psi}(x)\psi(x)]. \quad (15.9)$$

A ‘naive’ lattice formulation is obtained by replacing the derivatives by symmetric differences:

$$S_L^{\text{naive}} = \frac{1}{2\ell} \sum_{n,\mu} \bar{\psi}_n \gamma^\mu (\psi_{n+\mu} - \psi_{n-\mu}) + m \sum_n \bar{\psi}_n \psi_n. \tag{15.10}$$

The elementary solution of the associated dynamic equations, i.e., the propagator, is

$$\begin{aligned} G(p) &= \frac{\ell}{i\gamma^\mu \sin(p_\mu \ell) + m\ell} \\ &= \frac{-i\gamma^\mu \ell \sin(p_\mu \ell) + m\ell^2}{\sum_\mu \sin^2(p_\mu \ell) + m^2 \ell^2} \rightarrow \frac{1}{i\gamma^\mu p_\mu + m}. \end{aligned} \tag{15.11}$$

We identify the physical spectrum through the poles in the propagator at $p_0 = iE$:

$$\sinh^2(E\ell) = \sum_j \sin^2(p_j \ell) + m^2 \ell^2. \tag{15.12}$$

The lowest-energy solutions, as expected yielded for $p = (0, 0, 0)$ the usual $E \simeq \pm m$, but there are many other degenerate solutions yielding this value of E , at $\ell p = (\pi, 0, 0), (0, \pi, 0), \dots, (\pi, \pi, \pi)$. This is a model for 16 light fermions, not one. More generally, when fermions are discretized in this way on a d -dimensional lattice, they double and produce 2^d species.

Initially, two ways to deal with this problem were developed. The ‘Wilson fermions’ [273], and the ‘Kogut–Suskind (staggered) fermions’ [168]; more recently, also a five-dimensional formulation with ‘domain-wall fermions’ [155] has been considered. Wilson fermions are implemented by adding a second-derivative-like term,

$$S^W = -\frac{r}{2\ell} \sum_{n,\mu} \bar{\psi}_n (\psi_{n+\mu} - 2\psi_n + \psi_{n-\mu}), \tag{15.13}$$

to S^{naive} , Eq. (15.10). The parameter r must lie between 0 and 1; $r = 1$ is almost always used and ‘ $r = 1$ ’ is implied when one speaks of using ‘Wilson fermions’. The propagator is

$$G(p) = \frac{-i\gamma_\mu \sin(p_\mu \ell) + m\ell - r \sum_\mu [\cos(p_\mu \ell) - 1]}{\sum_\mu \sin^2(p_\mu \ell) + \left\{ m\ell - r \sum_\mu [\cos(p_\mu \ell) - 1] \right\}^2}. \tag{15.14}$$

It has one pair of ‘low-energy’ poles at $p_\mu \simeq (\pm im, 0, 0, 0)$. The other poles are at $p \simeq r/\ell$. In the continuum limit, these states become infinitely massive.

This makes all but one of the fermion species heavy (with heavy masses close to the cutoff $1/\ell$), and we have, in principle, the required discretization method. However, for the n_f flavor QCD addition of S^W , Eq. (15.13) breaks the $SU(n_f)_L \times SU(n_f)_R$ chiral symmetry; see section 3.3. The size of the symmetry breaking is proportional to the lattice spacing and only close to the continuum limit $\ell \rightarrow 0$ does the explicit chiral-symmetry breaking become small. At any finite lattice spacing a proper representation of the chiral symmetry of the massless theory becomes a subtle fine-tuning process.

Despite the computational problems related to implementation of chiral symmetry, there is also some advantage with this formulation. Wilson fermions are closest to the continuum formulation – there is a four-component spinor on every lattice site for every color and/or flavor of quark. Therefore, the usual rules apply to the formulation of currents, and states. Explicitly, the Wilson-fermion action for an interacting theory is

$$\ell S^W = \sum_n \bar{\Psi}_n \Psi_n - \kappa \sum_{n\mu} \left(\bar{\Psi}_n(r - \gamma_\mu) U_\mu(n) \Psi_{n+\mu} + \bar{\Psi}_n(r + \gamma_\mu) U_\mu^\dagger \Psi_{n-\mu} \right). \quad (15.15)$$

We have rescaled the fields $\psi = \sqrt{2\kappa}\Psi$, and have introduced the ‘hopping parameter’ $\kappa^{-1} = 2(m\ell + 4r)$.

In studies of properties of QGP, another description of quarks on a lattice has been used more extensively. In the staggered-fermion method, a one-component staggered-fermion field rather than the four-component Dirac spinors is used. The name staggered is used since Dirac spinors and quark flavors are constructed by combining appropriate single-component fields from different lattice sites. Staggered fermions also break the chiral symmetry, but there remains a $U(1) \times U(1)$ symmetry, which comprises much of the physics of chiral symmetry. Moreover, explicit chiral symmetry is present for $m_q \rightarrow 0$, even for finite lattice spacing, as long as all flavor masses are degenerate. On the other hand, flavor symmetry and translational symmetry are mixed together, which poses problems, since in the real world, the flavor symmetry is broken.

Since exact chiral symmetry and broken flavor symmetry are important physical phenomena influencing the physics of high-temperature QCD, see Fig. 3.4 on page 54, a third approach to place quarks on a lattice is currently being developed. The domain-wall formulation of lattice fermions is expected to support accurate chiral symmetry, even at finite lattice spacing. In this new fermion formulation, it seems that it will be possible to more easily simulate two-flavor, finite-temperature QCD near the chiral phase transition. For further theoretical details, we refer to [265], and the first exploratory hot-QCD calculations are reported in [90].

Another area of rapid development is the search for a most appropriate ‘improved’ action for each of the important applications of L-QCD. The original Wilson action for the gauge fields is not unique, since the principle of gauge invariance leads to the building block, the plaquette, but not to the actual form of the action made from plaquettes. Consequently, the form of Wilson-fermion action can also be ‘improved’. Improvements can perform better in one area than in another, since they address the problems encountered in extracting physics from extensive numerical calculations.

15.4 From action to results

Once we have quark fields on the lattice, as noted at the end of section 15.1, we must deal with their anticommuting nature. We carry out the integral over the Fermi fields in the path integral Eq. (15.4). For n_f degenerate flavors of staggered fermions

$$Z = \int [dU][d\psi][d\bar{\psi}] \exp\left(-\beta S(U) - \sum_{i=1}^{n_f} \bar{\psi} M(U) \psi\right) \quad (15.16)$$

$$= \int [dU] \left(\det M(U)\right)^{n_f/2} \exp(-\beta S(U)). \quad (15.17)$$

In order to make explicit the positive-definite nature of the Fermi determinant FD appearing as the preexponential factor in Eq. (15.17), we will be writing it as

$$FD = \det(M^\dagger M)^{n_f/4}.$$

Recalling that a determinant is a product of eigenvalues, we can express its logarithm as a sum of logarithms of eigenvalues, i.e., a trace, and we write

$$Z = \int [dU] \exp\left(-\beta S(U) - \frac{n_f}{4} \text{tr} \ln(M^\dagger M)\right). \quad (15.18)$$

The major computational problem dynamic fermion simulations face is inverting the fermion matrix M for any change in any of the gluon-link fields U . M has eigenvalues with a very large range – from 2π to $m_q \ell$ – and, in the physically interesting limit of small m_q , the matrix becomes ill-conditioned. Just a few years ago, it had been possible only to study quenched fermions, i.e., to proceed ignoring the second term in the exponent in Eq. (15.18). Today, it is possible to compute at relatively heavy values of the quark mass and to extrapolate to $m_q = 0$.

We will not enter further into practical discussion of how to do the high-dimensional Monte-Carlo integrals; neither shall we discuss the many

ingenious algorithms that are in use. This is clearly a field of its own merit, and would fill more than this volume. However, even if somebody did provide all numerical answers, we still would need to take a few further steps. Perhaps the most important physical consideration is the approach to the continuum limit, $\ell \rightarrow 0$. Any calculation by necessity will be done with a finite lattice spacing ℓ . The lattice spacing ℓ is an ultraviolet cutoff, and it is the variable which now provides the scale to the QCD coupling constant g and quark masses m_i .

The continuum limit, in which we are interested, requires the limit $\ell \rightarrow 0$, holding physical quantities fixed, not the input ('bare') action parameters. In section 14.3, we have shown that the input parameter g , the bare coupling of quantum chromodynamics, is replaced by the running coupling constant α_s measured at some given scale (typically M_Z). When only one dimensioned parameter is present, in the absence of quarks or when all quark masses are set to zero, the situation is simple. For example, in order to evaluate hadron masses on the lattice, one computes the dimensionless combination $\ell m(\ell)$. One can determine the physical meaning of the lattice spacing by fixing one hadron mass from experiment. Then other dimensional quantities can be predicted.

Consider, as an example, the ratio of two hadron masses:

$$\frac{\ell m_1(\ell)}{\ell m_2(\ell)} = \frac{m_1(0)}{m_2(0)} + \mathcal{O}(\ell) + \dots \quad (15.19)$$

The leading term does not depend on the value of the ultraviolet-cutoff. One of the goals of a lattice calculation aiming to obtain the physical properties is to separate an ultraviolet-cutoff-distance scale-dependent remainder from the physical observable. One says that the calculation 'scales' if the ℓ -dependent terms in Eq. (15.19) are zero or small enough that one can extrapolate to $\ell = 0$. All the ℓ -dependent terms are 'scale violations'. To be able to make extrapolations, the results for several values of lattice spacing ℓ are required.

The precision with which we can extract the physics will obviously depend on how small the lattice cutoff is. However, the lattice must cover a sufficiently large region of space-time for the physical question we are addressing. We cannot study the proton of size $R = 1$ fm without having a few lattice distances within its radius, and a lattice of a few fermis. Repeating this basic cell domain infinitely using periodic boundary conditions helps, but cannot much reduce these requirements.

A summary of the lattice-gauge-theory conditions and procedures which we have introduced is presented in table 15.1.

For the study of hadron masses, as long as fundamental symmetries are respected, the physical size of the lattice should be $\ell \simeq 0.1\text{--}0.2$ fm, and the repeating cell ought to have the size $\simeq 5$ fm. The computer power of today

Table 15.1. A summary of the procedure for L-QCD simulations

Do the path integral:
quark integrals analytically
gluon + Fermi-determinant integrals numerically
Restrictions:
Imaginary time
Chemical potential = 0
<i>quark-antiquark symmetry makes the determinant real</i>
Approximations:
Restrict volume $L \ll \infty$ (infrared cutoff)
Introduce lattice $\ell \geq 0$ (ultraviolet cutoff)
<i>Need: $\ell \ll l_{\text{typical}} \ll L$</i>
<i>limit: scale $\ell \rightarrow 0$</i>
Need low quark masses,
<i>Difficulty: $t_{\text{computer}} \sim (m_q)^{-2}$</i>
<i>limit: scale $m_q \rightarrow 0$</i>

allows $32^3 \times 16$, or $24^3 \times 48$, lattices. In view of the physical difference between time and space, the time, i.e., inverse-temperature, dimension of the lattice can be chosen to be smaller than the spatial extent of the lattice. On such lattices, the hadron spectra that emerge nowadays are quite realistic; see section 15.5 below.

However, such lattices may not be large enough to describe precisely many of the interesting properties of the QGP. We need to describe two different quark mass scales (u and d, and s) while maintaining chiral symmetry in the light-quark sector, and treating an odd number of quark flavors (both staggered and Wilson quarks favor the presence of an even number of flavors). This task has not been resolved completely, and the properties of QGP we will discuss retain a systematic uncertainty. Moreover, a many-body system such as QGP should have many collective modes of excitation. Given the size of the physical lattices studied, collective oscillations with wave lengths greater than a few fermis are not incorporated. Although this does not influence in a critical way the properties of the equations of state, such long-range oscillations are often carriers of flows, e.g., of heat. Therefore, the study of transport properties of the QGP phase on the lattice is not yet possible.

The euclidian lattice is indeed ideal for simulating high-temperature QCD since, in this case, there is a direct correspondence between the imaginary time and temperature – the path-integral weight is, in fact, the partition function with $\ell N_t = 1/T = \beta$. The statistical-physics prop-

erties are the operators which are fairly simple, e.g., the energy density involves only one point in space–time. One has to remember that other lattice studies of the hadron mass spectrum involve two point functions, whereas weak-interaction matrix-element computations typically involve three point functions since we have to create a hadron from the vacuum at $t = 0$, act on the state with an operator at $t = t_1$, and then annihilate the hadron at $t = t_2$.

Among the quantities which are studied in high-temperature QCD are the Polyakov loop [273], the chiral condensate $\bar{\psi}\psi$, Eq. (3.22), the energy and pressure, screening lengths of color-singlet sources, the potential between static test quarks, and the response of the quark density to an infinitesimal chemical potential. Of these, the Polyakov loop and $\bar{\psi}\psi$ are the most intensively studied. $\bar{\psi}\psi$ is the order parameter for chiral symmetry breaking. It is nonzero under ordinary conditions $T \rightarrow 0$, and we expect it to vanish when chiral symmetry is restored for $T > T_c$. Loosely speaking, the Polyakov loop has the value $e^{-F/T}$, where F is the free energy of a static test quark. In pure $SU_c(3)$ gauge QCD, the Polyakov loop is zero at low temperatures, indicating confinement of the test quark, and nonzero at high temperature.

It is understood today that dynamic quarks make a big difference in high-temperature QCD, and the ‘quenched’ approximation has been found to be in general unsuitable. Looking at the energy of free quarks and gluons (the Stefan–Boltzmann law, see section 4.6) even with $n_f = 2$ flavors of light quarks, we find that the $16 = 8_c \times 2_s$ gluon degrees of freedom are dominated by $21 = 2_f \times 3_c \times 2_s \times \frac{7}{4}$ equivalent quark degrees of freedom. The thermal properties of quarks dominate those of gluons. Quenched quarks are known to exclude the particle–antiparticle-pair fluctuations in the vacuum. Thus, if quenched quarks are used, some important physical processes are forbidden. For example, consider a quark–antiquark pair connected by a string of color flux. With quenched quarks, when the distance grows, we encounter an ever-growing linear potential – if pair fluctuations are excluded, this string never breaks. In the presence of dynamic quarks, when the string is long enough, there is enough energy to create a quark–antiquark pair, which breaks the string, forming two mesons.

It is easy to find, in the numerical Monte-Carlo integration, the transition (crossover) to some novel high-temperature behavior in a lattice simulation, though it is very difficult to ascertain the nature of the transition. To vary the temperature with a fixed number of lattice spacings in the time direction, the lattice spacing ℓ is changed by varying the coupling g . This works because g is the coupling constant defined on the scale of the lattice spacing. In an asymptotically free theory, the coupling decreases for shorter length scales. Therefore, decreasing

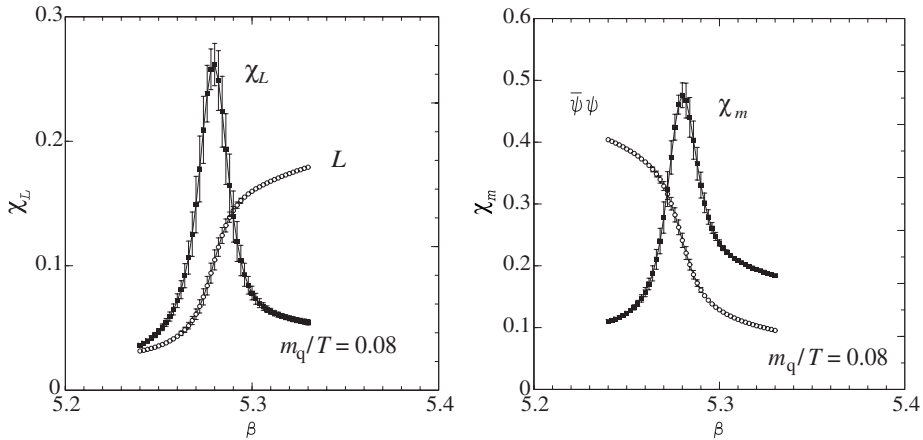


Fig. 15.1. Deconfinement and restoration of chiral symmetry in two-flavor L-QCD. Open circles: on the left-hand side the Polyakov loop L , which is the order parameter for deconfinement in the pure gauge limit ($m_q \rightarrow \infty$); and on the right-hand side quark chiral condensate $\bar{\psi}\psi$, which is the order parameter for chiral-symmetry breaking in the chiral limit ($m_q \rightarrow 0$), shown as a function of the coupling $\beta = 6/g^2$. Also shown are the corresponding susceptibilities $\chi_L \propto (\langle L^2 \rangle - \langle L \rangle^2)$ (left) and $\chi_m = \partial \langle \bar{\psi}\psi \rangle / \partial m$ (right) which peak at the same value of the coupling [159].

g , or increasing $6/g^2$ ($6 = 2n_c$), makes ℓ smaller and the temperature, $T = (N_t \ell(g))^{-1}$, higher. As the temperature is increased through the crossover, $\bar{\psi}\psi$ drops and the Polyakov loop increases, see Fig. 15.1. The Polyakov loop and $\bar{\psi}\psi$ change at the same temperature, indicating that ‘deconfinement’, and restoration of chiral symmetry are happening at the same temperature.

Little is known with certainty about the nature of the crossover between the confined (frozen) phase and the new phase suggested by Fig. 15.1. In particular, we cannot yet be sure what kind of phase transition or transformation is encountered, see Fig. 3.4 on page 54 and the related discussion. It is fairly well established, from lattice simulations, that there is a first-order phase transition in the pure gauge limit, and for three-massless quarks. As a quark mass is lowered from infinity this transition disappears, and there may be a continuous crossover from the low-temperature regime to the high-temperature regime. But even if there is no phase transition, the crossover is fairly sharp. This can be seen by considering the inverse screening lengths for $q\bar{q}$ sources with the quantum numbers of the pion π and its opposite-parity partner σ . At high temperatures, they become very close, with the remaining small difference being due to the explicit breaking of symmetry originating from the quark mass. This

and other quantities show that the high-temperature regime does indeed have the expected characteristics of the QGP.

Only recently have calculations progressed far enough to lead to firm results about properties of the QGP. To find the temperature of the crossover in physical units, the lattice spacing must be determined by computing some physical quantity, such as the ρ -meson or the nucleon masses. The π mass is not a good choice of scale, since it can be made arbitrarily small by making the quark mass small, as we have seen in section 3.3. Though the value of the crossover temperature one finds is still in doubt for real-life quarks, at present the opinion of experts we shall discuss in the next section is biased toward a value of 160 MeV [160], near the Hagedorn temperature; see chapter 12.

15.5 A survey of selected lattice results

There are many lattice results related to QCD properties we study, addressing diverse questions such as hadronic masses, matrix elements, and physical properties of hot QCD. Given the rapid development of the field which promises to render any presentation quite rapidly obsolete, we focus our attention on ‘stable’ results that are most relevant in the context of this book and, in particular, the study of equations of state of QGP. We will not further discuss in this section the intricate extrapolations (continuum limit, massless-quark limit) which form part of the process of evaluation of the bare numerical results, and which we described above in section 15.4.

The running of the gauge coupling constant has now been tested for the case of two massless Wilson fermions [76]. The lattice results compare very well with the renormalization-group result, as can be seen in Fig. 15.2. These results are, at present, still mainly of academic interest and are different in detail from Fig. 14.1, since, in the range $\alpha_s < 0.4$, we actually have to include s, c, and b quarks, in order to compare with experiment. On the other hand, the fact that the running is seen as expected in the theoretical evaluation of two-light-flavor QCD reassures us regarding the validity of the findings we presented in Fig. 14.1.

The study of hadronic masses allows one to draw conclusions about the input quark masses. The CP-PACS collaboration has recently completed an extensive evaluation using its dedicated (peak) 614-GFLOPS (giga-floating-point-operations) computer [33]. The lattice action and simulation parameters were chosen with a view to carrying out a precise extrapolation to the continuum limit, as well as scaling in the chiral $m_q \rightarrow 0$ limit for dynamic up- and down-quark masses. However, the strange quarks were considered in a quenched approximation, which entails an ‘uncontrolled’ error.

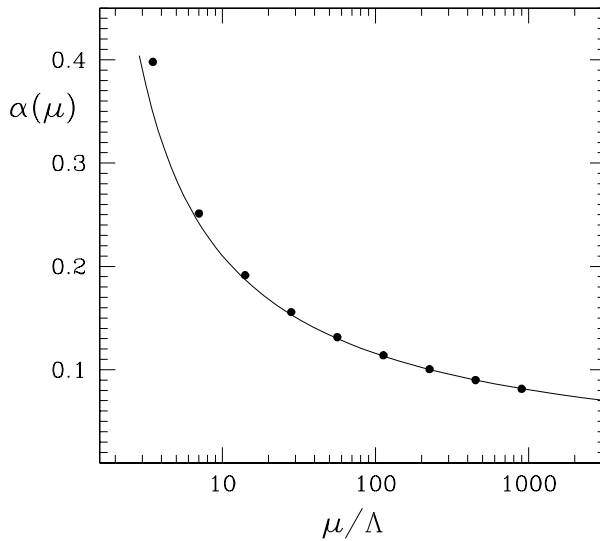


Fig. 15.2. Dots, lattice-gauge theory with two light fermions for $\alpha_s(\mu)$, compared with the perturbative three-loop result (line); parameters are chosen such that, for $\Lambda = 1$ GeV, $\alpha_s(M_Z) = 0.118$; results of the ALPHA collaboration [76].

Evaluation of the masses of kaons and/or ϕ allows one to determine the mass of the strange quark. The results found using dynamic u and d quarks are $m_s^{\overline{\text{MS}}}(2 \text{ GeV}) = 88_{-6}^{+4}$ MeV (K input) and $m_s^{\overline{\text{MS}}}(2 \text{ GeV}) = 90_{-11}^{+5}$ MeV (ϕ input), which are about 25% lower than the values found with quenched u and d quarks. The low value for the mass of the strange quark is well within the accepted range; see table 1.1 on page 7. The consistency of these two results is quite remarkable. Moreover, using the mass of the K meson to fix the strange-quark mass, the difference from experiment for the mass of the K^* meson is $0.7_{-1.7}^{+1.1}\%$, and that for the ϕ meson $1.3_{-2.5}^{+1.8}\%$. When the ϕ meson is used as input, the difference in the mass of the K^* meson is less than 1%, and that for the mass of the K meson is $1.3 \pm 5.3\%$. The masses of (multi)strange baryons are, within much larger computational error, also in agreement with the experimental values.

Should this relatively low mass for the strange quark be confirmed when dynamic strange quarks are introduced, the speed of production of strangeness at low temperatures $T \gtrsim T_c$ in QGP as perhaps formed at intermediate SPS energies would dramatically increase. Strangeness could develop into a highly sensitive ‘low energy’ probe of formation of QGP, even when the initial conditions reached are near to the critical temperature. In this context, it is interesting to note the steep rise and threshold of the strangeness-excitation function shown in Fig. 1.5 on page 17.

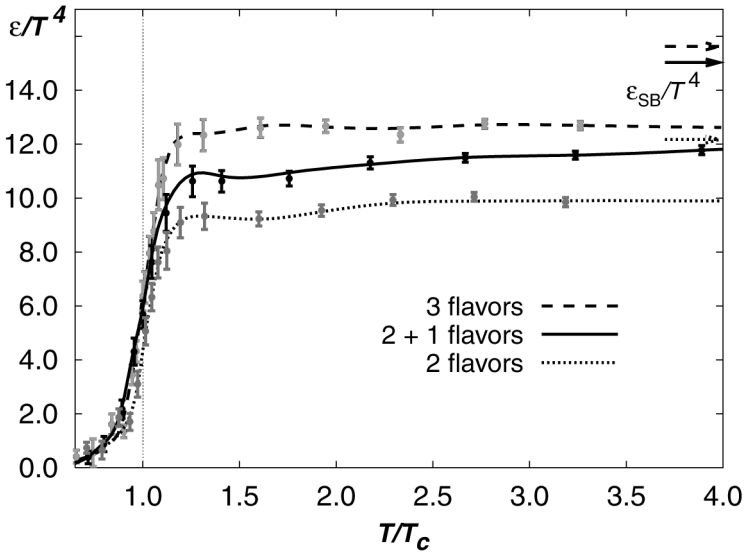


Fig. 15.3. The energy density of hadrons obtained with staggered fermions divided by T^4 , as a function of T/T_c . Stefan–Boltzmann limits of a non-interacting gas of quark and gluons are indicated with arrows for each case considered.

In our context, an even more important recent lattice advance has been the extensive study of 2, 2 + 1 and 3 flavors in hot QCD [159–161]. The behavior of the energy density ϵ/T^4 is presented in Fig. 15.3 as a function of temperature T/T_c , obtained with staggered fermions. The Stefan–Boltzmann values expected for asymptotically (high- T) free quarks and gluons are shown by arrows to the right, coded to the shades of the three results presented: two and three light flavors (up and down, respectively), for which the quark mass is $m_q = 0.4T$ and a third case (dark line), in which, in addition to the two light flavors, a heavier flavor $m_s = T$ is introduced. The temperature scale is expressed in units of the critical temperature T_c , as appropriate for each case (T_c changes with the number of flavors). The value of T_c is where one observes a rapid change in the behavior of the quark condensate/susceptibility and, at the same location, one sees also the onset of deconfinement in the Polyakov loop; see Fig. 15.1.

We see that, around $T/T_c = 1$, the number of active degrees of freedom rapidly rises, and the energy density attains as early as $T = 1.2T_c$ the behavior characteristic of an ideal gas of quarks and gluons, but with a somewhat reduced number of active degrees of freedom. The energy density in the deconfined phase can be well approximated by

$$\epsilon_{\text{QGP}} \simeq (11\text{--}12) T^4. \quad (15.20)$$

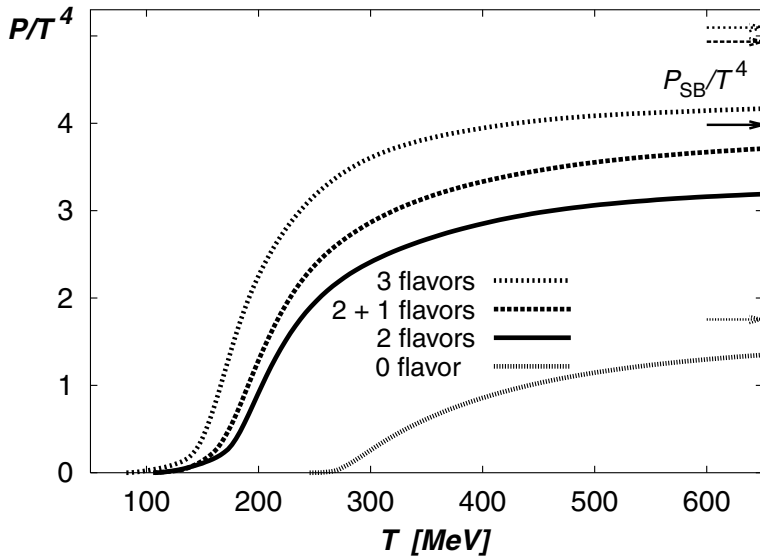


Fig. 15.4. The pressure of hadrons obtained with staggered fermions in units of T^4 as a function of T .

The critical temperature T_c has the value

$$\frac{T_c}{m_\rho} = 0.20 \pm 0.01, \quad T_c = 154 \pm 8 \text{ MeV}, \quad \text{for } n_f = 3, \quad (15.21)$$

where, in addition to the statistical error quoted above, a systematic error at a similar level, associated with uncertainties in the scaling behavior, is expected. In case of two flavors, the value $T_c = 173 \pm 8 \text{ MeV}$ is found. These results are consistent with calculations performed with clover-shape-improved Wilson action (see section 15.3) by the CP-PACS collaboration [32] for two flavors. In Fig. 15.4, we present the behavior of P/T^4 as a function of temperature, with the temperature scale derived from Eq. (15.21). The expected Stefan–Boltzmann limits are shown by arrows. Apart from the cases of 2, 2 + 1 and 3 flavors, we see also the ‘pure gauge’ case with zero flavors.

The conclusion we draw from these results is that the lattice-QCD evaluation has matured to the level of being able to offer information directly relevant to the physical properties of hot QCD. These results, in particular, show that there is a rapid phase transformation or even a first-order phase transition at $T_c = 163 \pm 15 \text{ MeV}$.

We see, in Fig. 15.4, that the phase-transition temperature decreases significantly with increasing number of flavors. However, the shapes of all curves scale similarly. This is shown in Fig. 15.5, in which the temperature scale is expressed in units of T_c and the pressure in terms of the ideal

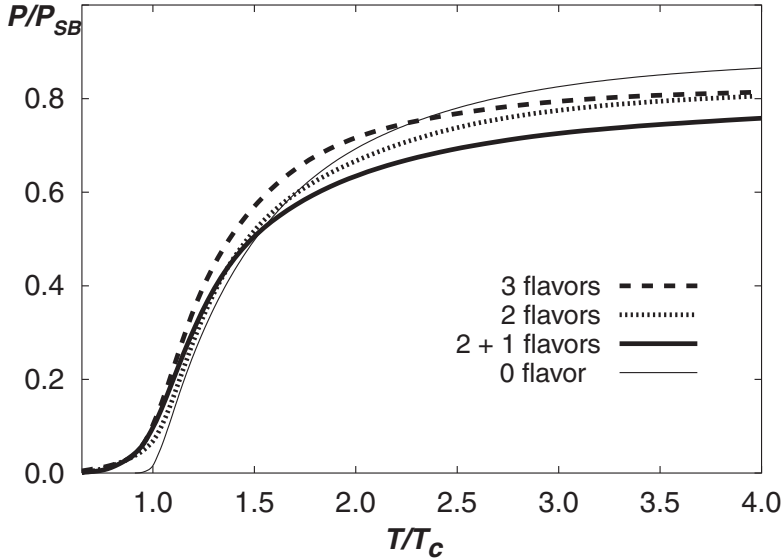


Fig. 15.5. The pressure of hadrons obtained with staggered fermions divided by the appropriate Stefan–Boltzmann limit, as a function of T/T_c .

Stefan–Boltzmann pressure. The zero-flavor pure gauge case is fastest growing toward the limiting value, but still at a considerably slower rate than that for the energy density we have seen in Fig. 15.3.

An ideal massless relativistic gas should satisfy the relation $\epsilon - 3P = 0$, Eq. (4.64). The difference in behavior, comparing Fig. 15.3 with Fig. 15.5, must originate from the presence of variables with dimensioned scales. We encountered two such (related) variables, the vacuum property \mathcal{B} and the parameter Λ controlling the magnitude of the running variables (α_s and m_i). The deviations of pressure from the Stefan–Boltzmann ideal-gas behavior seen in lattice results, in particular $\epsilon - 3P \neq 0$, are in direct or indirect fashion related to these quantities. We will quantify this in the following section.

We note that, using the Gibbs–Duham relation, Eq. (10.26), we can relate the change in the pressure, seen in Fig. 15.4, to the difference $\epsilon - 3P$. We generalize slightly the argument presented in Eqs. (4.62) and (4.64). We consider the free-energy density

$$f = -\frac{T}{V} \ln Z(T, V). \tag{15.22}$$

$P = -f$ for an infinite system. Moreover, the entropy density $\sigma = \partial/\partial T f$, see Eq. (10.6). We find, employing Eq. (10.26) at zero baryon density,

$$\frac{\epsilon - 3P}{T^4} = T \frac{d}{dT} \left(\frac{P}{T^4} \right). \tag{15.23}$$

As soon as we understand the gentle slope of pressure P in Fig. 15.4, i.e., the right-hand side of Eq. (15.23), we will also understand the difference between the behaviors of energy and pressure, the left-hand side of Eq. (15.23), noted on comparing Fig. 15.3 with Fig. 15.5.

We will show, in section 16.2, that this non-ideal-gas behavior can be interpreted as resulting from perturbative quark–gluon interactions and the presence of the latent heat of the vacuum \mathcal{B} . An equivalent explanation invoking the presence of quasi-particles with mass, and quantum numbers of quarks and gluons, will also be considered.

16 Perturbative quark–gluon plasma

16.1 An interacting quark–gluon gas

As explained in section 14.1, the interactions between quarks and gluons are contained in the QCD Lagrangian Eq. (13.79), improved by gauge-fixing and FP-ghost terms Eq. (14.1). Strictly considered, the rules for Feynman diagrams we presented in Eqs. (14.2)–(14.8) are applicable to processes in perturbative vacuum, whereas to compute thermal properties of interacting quark and gluons, we are working in matter at finite temperature T and chemical potential μ . The generalization required is discussed in detail in the textbook by Kapusta [157].

A lot of effort in the past few decades has gone into the development of the perturbative expansion of the partition function. The series expansion, in terms of the QCD coupling constant g , has been carried out to order $[(g/(4\pi))^5 = (\alpha_s/\pi)^{5/2}/32$ [282]. This series expansion, which was developed using as reference the perturbative vacuum in empty space, does not appear to lead to a convergent result for the range of temperatures of interest to us [36]: the thermodynamic properties vary widely from order to order, oscillating quite strongly around the Stefan–Boltzmann limit. It has therefore been claimed that the perturbative QCD thermal expansion has a zero-range convergence radius in α_s .

Our following considerations will be limited to the lowest-order perturbative term combined with the vacuum energy \mathcal{B} and allow an excellent reproduction of the key features of lattice results. It remains to be understood why this is the case. It is not uncommon to encounter in a perturbative expansion a semi-convergent series. The issue then is how to establish a workable scheme. It is, for example, possible that a different scheme of perturbative approach, in which the QCD parameters (α_s and masses) are made nonperturbative functions of the medium using an in-medium renormalization group, would yield a better converging series in α_s .

Considering the inconclusive and rapidly evolving landscape of thermal